Journal of Pharmaceutical Analysis 15 (2025) 101108

Contents lists available at ScienceDirect

Journal of Pharmaceutical Analysis

journal homepage: www.elsevier.com/locate/jpa

Original article

Photoaffinity probe-enabled discovery of sennoside A reductase in *Bifidobacterium pseudocatenulatum*

Yang Xu [1], Shujing Lv [1], Xiang Li [1], Chuanjia Zhai, Yulian Shi, Xuejiao Li, Zhiyang Feng, Gan Luo, Ying Wang **, Xiaoyan Gao *

School of Chinese Materia Medica, Beijing University of Chinese Medicine, Beijing, 102488, China

ARTICLE INFO

Article history:
Received 15 April 2024
Received in revised form
29 August 2024
Accepted 18 September 2024
Available online 21 September 2024

Keywords:
Reductase
Sennoside A
Photoaffinity labeling
Gut bacteria
Transformation
Chemical biology
Small molecule

ABSTRACT

Sennoside A (SA), a typical prodrug, exerts its laxative effect only after its transformation into rheinanthrone catalyzed by gut microbial hydrolases and reductases. Hydrolases have been identified, but reductases remain unknown. By linking a photoreactive group to the SA scaffold, we synthesized a photoaffinity probe to covalently label SA reductases and identified SA reductases using activity-based protein profiling (ABPP). From lysates of an active strain, *Bifidobacterium pseudocatenulatum* (*B. pseudocatenulatum*), 397 proteins were enriched and subsequently identified using mass spectrometry (MS). Among these proteins, chromate reductase/nicotinamide adenine dinucleotide (NADH) phosphate (NADPH)-dependent flavin mononucleotide (FMN) reductase/oxygen-insensitive NADPH nitroreductase (nfrA) was identified as a potent SA reductase through further bioinformatic analysis and The Universal Protein Resource (UniProt) database screening. We also determined that recombinant nfrA could reduce SA. Our study contributes to further illuminating mechanisms of SA transformation to rheinanthrone and simultaneously offers an effective method to identify gut bacterial reductases.

1. Introduction

The gut microbiome is a complex microbial community in the human gastrointestinal tract and regulates the biotransformation of oral medicines via intestinal bacterial enzymes, including hydrolases, lyases, oxidoreductases and transferases [1–3]. The number of gut bacteria in the human intestine is 10^{14}, which is 10 times greater than that of human cells, and genes encoded by the community are 100 times greater than those in the human genome [4,5]. Because of their wide diversity and abundance, they pose great challenges to the identification of drug metabolic enzymes, which are still in their infancy [6]. In addition, previous studies have shown that although enzyme genes with specific metabolic functions tend to be widely distributed in gut bacteria, the strains are less distributed than their genes [7]. Therefore, to improve the accuracy of identifying unknown metabolic enzymes, researchers generally first select single strains with metabolic activity from the complex intestinal flora and determine the metabolic enzymes [8,9].

In an anaerobic intestinal microenvironment, commensal gut bacteria principally participate in hydrolysis reactions and reductive biotransformation of drugs [10]. Many studies have focused on the identification of gut bacterial hydrolases to elucidate the mechanisms of drug action, with fewer reports on reductases. Thus, there is an urgent need to identify metabolic reductases in the intestine comprehensively and accurately.

Traditional methods for identifying drug metabolic enzymes include genomic analysis, transcriptomics analysis [11], proteomics analysis [12], mining based on homologous enzymes [13], and so on [14]. Such methods offer information regarding enzyme abundances but limited insight into enzyme activities under specific conditions. Activity-based protein profiling (ABPP) uses activity-based probes (ABPs) to covalently label active site residues in the binding pockets of specific enzyme families to monitor enzymatic functions in complex biological systems [15,16]. For example, Cravatt and co-workers [17] designed a series of fluorophosphate-based probes to covalently label active serine residues of the catalytic triad (Ser-His-Asp (or Glu)) in serine hydrolases, thereby uncovering numerous functionally unannotated

* Corresponding author.
** Corresponding author.
E-mail addresses: gaoxiaoyan@bucm.edu.cn (X. Gao), wangy174@126.com (Y. Wang).
Peer review under responsibility of Xi'an Jiaotong University.
[1] These authors contributed equally to this work.

https://doi.org/10.1016/j.jpha.2024.101108

serine hydrolases. Interestingly, ABPP also has been applied to explore intestinal bacterial hydrolases and oxidases, but rarely to reductases, perhaps because of the lack of conserved amino acid residues in the binding pockets of reductases [18]. As reductases have distinct nucleophilic groups responsible for their catalytic function in the binding pockets, it is challenging to use ABPs to covalently label active site residues of unknown reductases based on known members of the reductase family. Recently, photoreactive groups have been reported to covalently react with amino acid residues of proteins when exposed to specific ultraviolet (UV) light [19,20]. For example, Xiao and co-workers [21] designed a photoaffinity probe ST-Dayne to identify uridine diphosphate (UDP)-glycosyltransferases in *Arabidopsis thaliana* and found UGT73C1 as a steviol-catalyzing UDP-glycosyltransferase. Accordingly, the incorporation of the photoreactive groups into ABPs will show great advantages in excavating unannotated reductases, and relative reports are few.

Sennoside A (SA), a natural active dianthrone in *Radix* et *Rhizoma Rhei* and *Sennae Folium*, exerts laxative effects after being transformed into an active component, rheinanthrone, under the catalysis of intestinal bacterial enzymes via two main pathways [22–24]. One of the two metabolic pathways is that SA transforms to sennidin A and later rheinanthrone catalyzed by hydrolases and reductases, respectively [25–28]. The other is that SA is reduced first and then catalyzed [29,30]. Many studies have proven that the hydrolases are β-glucosidases, and only one study has suggested that SA reductases could be nicotinamide adenine dinucleotide (NADH)/NADH phosphate (NADPH)-flavin reductases. The reductases remain unidentified. Here, we designed a photoaffinity probe based on SA (SAP) to identify SA reductases in *Bifidobacterium pseudocatenulatum* (*B. pseudocatenulatum*) (Scheme 1A). Diaziridine was selected as the photoreactive group for labeling proximal residues in SA reductase active sites, followed by UV irradiation [31,32]. The labeled proteins were enriched and further identified using mass spectrum-based proteomic analysis (Scheme 1B). Among the identified 397 proteins, chromate reductase/NADPH-dependent flavin mononucleotide (FMN) reductase/oxygen-insensitive NADPH nitroreductase (nfrA) was inferred as a potent SA reductase. Then, a three-dimensional (3D) model of nfrA was constructed and molecular docking was performed to investigate possible interactions between nfrA and SA. More importantly, nfrA was expressed in an *Escherichia coli* (*E. coli*) system, purified, and then incubated with SA to validate its catalytic activity. This study contributes to a deeper understanding of the metabolic pathways of SA and provides a powerful reference to identify reductases in intestinal bacteria.

2. Materials and methods

2.1. Materials

N-hydroxysuccinimide, *N*,*N*′-dicyclohexylcarbodiimide, *N*,*N*-diisopropylethylamine, glutathione (reduced), 1,4-dithiothreitol (DTT), and L-cysteine were obtained from Shanghai Aladdin Biochemical Technology Co., Ltd. (Shanghai, China). L-ascorbic acid was obtained from Beijing Chemical Works (Beijing, China). SA was obtained from Shanghai Yuanye Bio-Technology Co., Ltd. (Shanghai, China). 2-(3-(But-3-yn-1-yl)-3*H*-diazirin-3-yl)ethan-L-amine was obtained from Shanghai Acmec Biochemical Co., Ltd. (Shanghai, China). Dimethylformamide (DMF) and methanol (ananlytical grade) was obtained from Tianjin Zhiyuan Chemical Reagent Co., Ltd. (Tianjin, China). Isopropyl alcohol (high performance liquid chromatography (HPLC) grade), methanol (HPLC grade), formic acid (HPLC grade), acetonitrile (liquid chromatography-mass spectrometry (LC-MS) grade), methanol (LC-MS grade), formic acid (LC-MS grade), and protein marker (10–170 kDa) were obtained from Thermo Fisher Scientific Inc. (Waltham, MA, USA). Watsons Water (pure distilled) was obtained from Guangzhou Watsons Food and Beverage Co., Ltd (Guangzhou, China). Human NAD(P)H quinone dehydrogenase 1 (hNQO1), FMN-Na, and isopropyl β-D-thiogalactoside (IPTG) was obtained from Merck KGaA (Darmstadt, Germany). Emodin was obtained from Chengdu Biopurify Technology Development Co., Ltd. (Chengdu, China). Sodium bicarbonate was obtained from Fuchen Chemical Reagent Co., Ltd. (Tianjin, China). *Tert*-butanol (tBuOH), *N*,*N*-dimethyl-4-nitrosoaniline, Tris[(1-benzyl-1H-1,2,3-triazol-4-yl)methyl]amine (TBTA), and acetic acid were obtained from Shanghai Macklin Biochemical Technology Co., Ltd. (Shanghai, China). Dimethyl sulfoxide (DMSO) was obtained from Damao Chemical Reagent Factory (Tianjin, China). Phosphate-buffered saline (PBS), Coomassie brilliant blue (CBB) staining solution, bicinchoninic acid (BCA) protein assay kit, BeyoMag™ Streptavidin Magnetic Beads, and Tween-20 were obtained from Beyotime Biotechnology (Shanghai, China). 30% acrylamide-bisacrylamide (Acr-Bis) (29:1, *m*/*m*), sodium dodecyl sulfate-polyacrylamide gel electrophoresis (SDS-PAGE) separating gel buffer (4×, pH 8.8), SDS-PAGE concentration gel buffer (4×, pH 6.8), and Tris (5×) glycine electrophoresis buffer were obtained from Jiaxing Aiqi Biotechnology Co., Ltd. (Jiaxing, China). The 96-well plate was obtained from Corning Inc. (Corning, NY 14831, USA). Ammonium persulfate and loading buffer (5×) were obtained from Applygen Technologies Inc. (Beijing, China). Bacterial protein preparation lysate (with Tris-HCl) was obtained from Sangon Biotech Co., Ltd. (Shanghai, China).

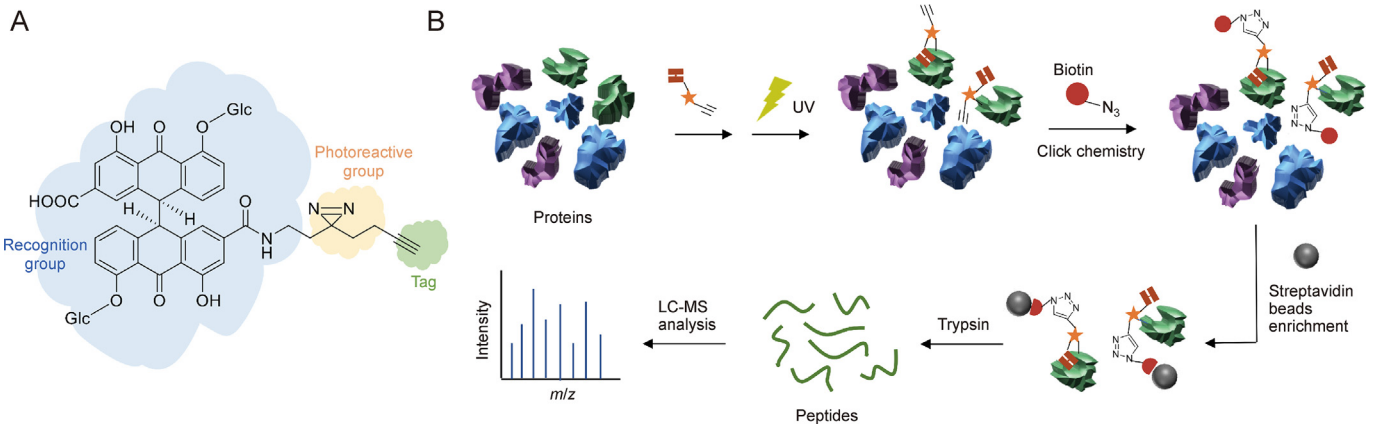

Scheme 1. Activity-based protein profiling (ABPP) was used to probe sennoside A (SA) reductases. (A) Structure of the photoaffinity probe based on SA (SAP). (B) Workflow of probing SA reductases using ABPP. UV: ultraviolet; LC-MS: liquid chromatography-mass spectrometry.

Iodoacetamide (IAA), tris(2-carboxyethyl)phosphine (TCEP), ammonium bicarbonate, and *N*,*N*,*N*′,*N*′-tetramethylethylenediamine were obtained from Sigma-Aldrich (Shanghai) Trading Co., Ltd. (Shanghai, China). Sequencing grade modified trypsin was obtained from Promega (Beijing) Biotech Co., Ltd. (Beijing, China). NADH and NADPH-Na_4 were obtained from Beijing Solarbio Science & Technology Co., Ltd. (Beijing, China). Kanamycin was obtained from Beijing Pulilai Gene Technology Co., Ltd. (Beijing, China). *E. coli* BL21-CodonPlus (DE3)-RIL competent cell was obtained from Beijing Biomed Gene Technology Co., Ltd. (Beijing, China). Tris-HCL and Luria-Bertani (LB) agar were obtained from Beijing BioDee Biotechnology Co., Ltd. (Beijing, China). *Bifidobacterium longum* (BeNa Culture Collection (BNCC) 186483), *Bifidobacterium breve* (BNCC 185972), *Bifidobacterium adolesentis* (BNCC 186535), *B. pseudocatenulatum* (BNCC 134343), *Clostridium butyricum* (BNCC 337239), *Clostridium perfringens* (BNCC 185933), *Lactobacillus brevis* (BNCC 337373), *Lactobacillus acidophilus* (BNCC 336636), and *Lactobacillus fermentum* (BNCC 194390) were purchased from BeNa Culture Collection Biotechnology Co., Ltd. (Beijing, China).

2.2. Animals

Institute of Cancer Research (ICR) mice (18−22 g) were supplied by SPF (Beijing) Biotechnology Co., Ltd. (Beijing, China). The animals were kept under controlled environmental conditions (a 12 h light/12 h dark cycle, a temperature of 20 ± 2 °C, and humidity of 60% ± 5%) with free access to food and water for three days prior to the commencement of the experiments. All animal experiments were approved by the Animal Ethics Committee of the Beijing University of Chinese Medicine (Beijing, China) (Approval No.: BUCM-4-2018091304-3023), and all procedures were performed in accordance with institutional guidelines and ethical standards.

2.3. Incubation with SA/SAP

2.3.1. Incubation of common reductants with SA

SA was added to the reaction solution containing glutathione, NADH, ascorbic acid, DTT, and L-cysteine (at a concentration of 1 mM) to a final concentration of 0.2 mg/mL. The mixtures were incubated at 37 °C for 24 h under anaerobic conditions. At the same time, the control group and blank group were set up. The control group did not contain reductants, and the blank group did not contain SA solution. Each group was conducted in triplicate. After processing the incubated samples, the supernatants were subjected to the ultra-high performance liquid chromatography-quadrupole time-of-flight mass spectrometry (UPLC-Q-TOF/MS) system.

2.3.2. Incubation of gut bacteria strains with SA

Gut bacteria, such as strains *Bifidobacterium longum*, *Bifidobacterium breve*, *Bifidobacterium adolesentis*, *B. pseudocatenulatum*, *Clostridium butyricum*, *Clostridium perfringens*, *Lactobacillus brevis*, *Lactobacillus acidophilus*, and *Lactobacillus fermentum,* were transferred into a conical flask containing Gifu anaerobic medium (GAM). The growth state of the bacteria was determined by measuring the optical density at 600 nm (OD_{600}). At an OD_{600} value of 0.8, the bacterial cultures were collected for the experiment. SA was incubated with 900 μL of gut bacteria cultures at a final concentration of 0.2 mg/mL at 37 °C for 24 h under anaerobic conditions. At the same time, the control group and the blank group were established. The control group did not contain intestinal strain cultures, and the blank group did not contain SA solution. Each group was conducted in triplicate in parallel. After processing the incubated samples, the supernatants were subjected to the UPLC-Q-TOF/MS system.

Dicoumarol (DIC) was reported as an active inhibitor of hNQO1. The gut bacteria strain/human gut microbiota suspension (100 μL) and SA solution (1 mg/mL, 100 μL) were added to 800 μL of GAM. DIC was added to the incubation system at final concentrations of 25, 50, and 100 μM. The mixtures were incubated at 37 °C for 24 h under anaerobic conditions. The control group was not treated without DIC. Each group was conducted in triplicate in parallel. After processing the incubated samples, the supernatants were subjected to the UPLC-quadrupole-linear ion trap MS (UPLC-QTRAP-MS/MS) system to detect the azomethine derivatives of the reductive metabolites of SA.

2.3.3. Incubation of hNQO1 with SA

The reaction mixture consisted of SA (200 μM), hNQO1 (10 μM), and NADH (400 μM) in PBS (pH 7.4, 0.01 M) at a final volume of 320 μL under an anaerobic environment. The reaction was terminated after 24 h. The control group was treated without hNQO1. Each group was performed in triplicate in parallel. Samples were collected at predetermined time intervals of 0.5, 1, 4, 6, and 12 h. After processing the incubated samples, the organic layer was taken out to detect whether there were reductive metabolites of SA by the UPLC-Q-Exactive Orbitrap-MS system.

The inhibitor reaction system comprised 10 μL of DIC, 4.65 μL of hNQO1, and 265.35 of μL PBS. The system was preincubated for 30 min, and then SA (1 mM) and NADH (2 mM) were added to activate the reaction. The system was mixed evenly and incubated in an anaerobic environment at 37 °C for 24 h. In the inhibitor control group, DMSO, which is a blank solvent of the same volume of inhibitor, was added. At the same time, a control group without hNQO1 was set and supplemented with PBS to the same total volume. Each group was conducted in triplicate in parallel. After processing the incubated samples, the supernatants were subjected to the UPLC-QTRAP-MS/MS system.

2.3.4. Incubation of hNQO1 with SAP

The experiment was performed in accordance with the experiment mentioned in Section 2.3.3, expect the substitution of the SA solution (4 μL) with SAP solution (4 μL; 1 mg of SAP was dissolved in 1 mL of DMSO and the solution was filtered) in the experimental group. In addition, samples were collected at predetermined time intervals of 0.5 and 12 h.

2.3.5. Incubation of ovalbumin (OVA) with SAP

Four groups were set to explore the capacity of SAP to covalently label proteins. The experimental group included an OVA solution (90 μL; 2.5 mg of OVA was dissolved in 1 mL of PBS solution and stored at −20 °C) and SAP solution (10 μL). A control group without SAP was also established, comprising an OVA solution (45 μL) and a DMSO solution (5 μL). A PBS solution (50 μL) was used as a cyanine5 azide control. In another group, an OVA solution (20 μL) and a PBS solution (50 μL) were combined. The four groups were incubated in the dark at room temperature for 1 h.

The OVA-SAP mixture (100 μL) was divided into two groups equally: one group and other groups mentioned above were irradiated using a 16 W UV lamp at 365 nm for 10 min; the other group without UV light irradiation was used as a control group.

To complex Cu^{2+} with ligands to avoid denaturing proteins in the samples, cyanine5 azide (0.601 mg of cyanine5 azide was dissolved in 1 mL of DMSO), TCEP (28.665 mg of TCEP was dissolved in 1 mL of H_2O), TBTA (5.3 mg of TBTA was dissolved in 1 mL of tBuOH/DMSO (1:4, *V*/*V*)) and $CuSO_4$ (15.961 mg of $CuSO_4$ was dissolved in 1 mL of ddH_2O) solutions were mixed in advance. The mixed solution was added to each group, except the OVA group, to perform a click chemistry reaction, and the mixture was incubated in the dark at 37 °C for 1 h. The final concentrations of cyanine5 azide, TCEP, TBTA, and $CuSO_4$ in the system were 100 μM, 1 mM, 100 μM, and 1 mM, respectively.

A loading buffer (5×) was added to each group, and all groups were boiled at 95 °C for 5 min. The samples were separated by 12% SDS-PAGE. The separation gels were stained with CBB to show the actual amounts of proteins in each lane.

2.3.6. Incubation of nfrA with SAP

A nfrA solution was added with SA solution, FMN-Na, and NAPDH, and incubated for 24 h in an anaerobic environment at 37 °C. The final concentration of SA, FMN-Na, and NAPDH in the system was 0.1 mM. A control group without nfrA was set. The experimental group and the control group were both conducted in triplicate. Here, 45 μL of the sample was collected at time intervals of 0.5, 1, and 4 h. After processing the incubated samples, the upper organic phase was analyzed by the UPLC-Q-Exactive-Orbitrap-MS system to quantify the derivatives of 8-glucosylrheinanthrone in each group.

2.4. Sample pretreatment before LC-MS/MS detection

The incubation reaction was terminated at each time point with 10% acetic acid and an equal volume of ethyl acetate. Then, 0.1 mL of 1% *N*,*N*′-dimethyl-4-nitrosoaniline dissolved in methanol was added, mixed, and set for 10 min. For samples to be quantified, an equal volume of acetonitrile containing 10 μg/mL 1,8-dihydroxyanthraquinone was added to the incubation system. The samples were centrifuged at 12,000 rpm for 10 min at 4 °C. The supernatants were subjected to LC-MS/MS analysis.

2.5. Administration of an inducer, inhibitor, SA, and sample collection

Butylated hydroxyanisole (BHA) is an effective inducer of NAD(P)H:quinone oxidoreductase (NQO) [33]. Sixteen ICR mice were randomly divided into the BHA-pretreated group and control group I ($n = 8$ for each group). Mice in the BHA-pretreated group were orally treated with BHA (600 mg/kg) suspended in corn oil twice daily for 10 days. Control group I mice were treated orally with an equivalent amount of corn oil. Stools were collected on day 10 to determine the activity of NQO in the gut microbiota. Meanwhile, two groups of mice received a single dose of SA (50 mg/kg). Total stool grains, loose stool grade, loose stool rate, and diarrhea index were used to evaluate the difference in the laxative effect of SA on the mice.

Another 16 ICR mice were randomly divided into the DIC-pretreated group and control group I ($n = 8$ for each group). Mice in the DIC-pretreated group were treated orally with DIC (30 mg/kg) suspended in corn oil once daily for five days. Mice in the control group I were treated orally with an equivalent amount of corn oil. Stools were collected on day 5 to determine the activity of NQO in the gut microbiota. Meanwhile, two groups of mice received a single dose of SA (50 mg/kg). Total stool grains, loose stool grade, loose stool rate and diarrhea index were used to evaluate the difference in the laxative effect of SA on the mice.

2.6. Evaluation method of diarrhea effect

The ICR mice treated with SA were immediately placed in a metabolic cage with white filter paper on the bottom. These mice were fasted but allowed to drink water within 24 h. The following indicators were observed.

1) Number of stool grains: the total number of stool grains passed per animal.
2) Loose stool grade: indicating the degree of loose stool. The loose stool grade was determined using the size of the stained area of loose stool on the filter paper. It was divided into four grades: grade 1 (<1 cm), grade 2 (1–1.9 cm), grade 3 (2–3 cm), and grade 4 (>3 cm). In statistics, the series of each pile of dilute stool is counted individually, and then the average dilute stool series is obtained by dividing all dilute stool series of the rat.
3) Loose stool rate: the ratio of the number of loose stools to the total number of stool grains per animal.
4) Calculation of diarrhea index: the diarrhea index of each mouse was calculated as the product of loose stool grade and loose stool rate.

In addition, to reduce human error in statistics, the experiment unified rules were the following: 1) if we could not distinguish the number of a pile of fecal grains, it was counted as one. 2) The filter paper was used as a standard to distinguish between dilute and dry stool. 3) Serial diameter measurement: circle one to measure its diameter, ellipse, or irregular one to measure its longest and approximate circle diameter and divide the sum of two numbers by 2). 4) Observation time: within 5 h after administration.

2.7. Synthesis of SAP

SA (100.0 mg, 0.116 mmol), *N*,*N*′-dicyclohexyl carbodiimide (24.0 mg, 0.116 mmol), and *N*-hydroxysuccinimide (26.8 mg, 0.24 mmol) were dissolved in DMF (4 mL) and stirred at room temperature for 12 h. The reaction was performed under nitrogen away from light. Then 2-(3-(but-3-yn-1-yl)-3*H*-diazirin-3-yl) ethan-1-amine (7.96 mg, 0.058 mmol) and *N*,*N*′-diisopropylethylamine (60.6 μL, 0.348 mmol) were added to the system and allowed to react for 2 h. HPLC was used to monitor in real time whether products were produced.

The products were redissolved in methanol/water mixtures and purified by flash chromatography, and the solvents were removed using a rotary evaporator. The products were transformed from liquid to solid after freeze-drying and vacuum-drying. The structure of the purified products was characterized by nuclear magnetic resonance spectroscopy (NMR) and high-resolution MS (HRMS): ^{1}H NMR (400 MHz, DMSO-d_6) δ 7.96 (s, 1*H*), 6.85 (d, $J = 7.7$ Hz, 2*H*), 6.80 (s, 1H), 6.72 (d, $J = 8.4$ Hz, 2*H*), 6.62 (s, 1*H*), 6.39 (dd, $J = 22.7$, 7.9 Hz, 4*H*), 5.35–4.44 (m, 14*H*), 3.99–3.10 (m, 10*H*), 2.90 (t, $J = 7.1$ Hz, 2*H*), 2.78 (s, 1*H*), 1.94 (t, 2*H*), 1.51 (q, $J = 7.6$ Hz, 4*H*); ^{13}C NMR (400 MHz, DMSO-d_6) δ 12.70, 25.25, 27.32, 31.35, 31.89, 34.23, 40.43, 52.85, 57.67, 60.95, 61.15, 70.07, 71.80, 74.25, 74.28, 74.30, 76.15, 76.21, 77.64, 77.71, 83.23, 102.38, 102.49, 106.72, 106.87, 112.43, 114.47, 115.44, 117.17, 118.83, 118.92, 124.88, 124.95, 134.93, 134.76, 135.97, 136.10, 146.05, 149.19, 158.98, 159.07, 164.62, 164.64, 167.07, 167.48, and 192.58. HRMS: $[M-H]^-$ calculated for $C_{49}H_{47}N_3O_{19}$: 980.2720, found: 980.2720.

2.8. LC-MS/MS detection of SA-derived metabolites

2.8.1. UPLC-Q-TOF/MS analysis

UPLC analysis was performed on a Waters ACQUITY™ I-Class system (Waters, Milford, MA, USA) consisting of a binary solvent system, an autosampler, and a column temperature controller. Chromatographic separation was carried out on an ACQUITY BEH C_{18} column (2.1 mm × 100 mm, 1.7 μm, Waters). The mobile phase was composed of eluent A (0.1% formic acid in water) and eluent B (acetonitrile). The line gradient program was optimized as follows: 0–8 min, 5%–55% B; 8–11 min, 55%–65% B; 11–12.5 min, 65%–95% B; 12.5–13 min, 95%–5% B; and 13–15 min, 5% B. Column temperature was set to 40 °C. Sample chamber temperature was set to 4 °C. The mobile phase flow rate was set to 0.2 mL/min and the injection volume was 2 μL for each run. MS analysis was performed on a Waters SYNAPT G2-SI MS system equipped with an

electrospray ionization source. Analysis was performed in negative ion mode. The source parameters were set as follows: capillary voltage, 3.0 kV; cone voltage, 40 V; source temperature, 100 °C; desolvation temperature, 400 °C; cone gas flow, 50 L/h; and desolvation gas flow, 800 L/h. The low collision energy was 6 eV and the high collision energy was 10–65 eV. Mass spectra were recorded across the range *m/z* 50–1200 and 3D data were collected in continuum mode. Leucine-enkephalin was used as the lock mass solution, generating an $[M-H]^-$ ion (*m/z* 554.2615) to ensure accuracy during MS analysis. MS data were acquired and processed using Waters MassLynx V4.1 software.

2.8.2. UPLC-QTRAP-MS/MS analysis

LC analysis was performed on a Prominence LC-20A system (Shimadzu, Kyoto, Japan) consisting of a binary solvent system, an autosampler and a column temperature controller. Chromatographic separation was performed on a Waters ACQUITY™ UPLC HSS T3 column (2.1 mm × 100 mm, 1.8 μm). The mobile phase was composed of eluent A (0.1% formic acid in water) and eluent B (acetonitrile). The line gradient program was optimized as follows: 0–0.1 min, 5% B; 0.10–1 min, 5%–20% B; 1–7 min, 20%–70% B; 7–8 min, 70%–100% B; 8–8.1 min, 100%–5% B; and 8.1–10.5 min, 5% B. The column temperature was set to 40 °C. The sample chamber temperature was set to 15 °C. The mobile phase flow rate was set to 0.3 mL/min and the injection volume was 3 μL for each run. MS data were recorded using AB SCIEX QTRAP 5500 (Framingham, MA, USA). MS spectrometric analyses were conducted using an electrospray ionization source in negative ion mode. The mass spectrometric parameters were optimized as follows: ion spray voltage, −4500 V; source temperature, 650 °C; curtain gas, 30 L/min; ion source gas 1, 55 L/min; and ion source gas 2, 60 L/min. MS/MS conditions were optimized for the internal standard by injecting the individual solution into the electrospray source. The parameters were optimized in multiple reaction monitoring (MRM) mode to achieve the highest possible sensitivity. The MS parameters of the compounds are shown in Table 1.

2.8.3. UPLC-Q-Exactive-Orbitrap-MS analysis

UPLC data were acquired using the Ultimate 3000 UHPLC system. The column was an ACQUITY UPLC BEH C_{18} column (2.1 mm × 100 mm, 1.8 μm) and maintained at 38 °C. A gradient was established using mobile phases A (0.1% formic acid in aqueous solution) and B (acetonitrile). In the experiment in Section 2.3.3, the solvent gradient was set as follows: 0–2 min, 11% B; 2–5.1 min, 11%–14% B; 5–5.1 min, 14%–25% B; 5.1–7.5 min, 25% B; 7.5–8 min, 25%–40% B; 8–14 min, 40% B; 14–16 min, 40%–100% B; 16–18 min, 100% B; 18–18.5 min, 100%–11% B; and 18.5–20 min, 11% B. The flow rate of the mobile phases was 0.3 mL/min. The temperature of the sample chamber was 4 °C. We used electron spray ionization to ionize samples with a spray voltage set to 3200 V and performed detection using parallel reaction monitoring in negative ion mode. Because of the different signals of different metabolites, we optimized the normalized collision energies of the different metabolites: azomethyl derivative of 8-glucosylrheinanthrone, 20%; rhein-8-*O*-β-D-glucoside, 20%; and emodin, 50%. Some other parameters are listed as follows: capillary temperature, 350 °C; sheath gas, 35 (arbitrary units); auxiliary gas, 15 (arbitrary units); mass resolution, 17,500; AGC target, 2×10^5; isolation window, 1.0 *m/z* units; and maximum IT, 100 ms.

In the experiment in Section 2.3.2, the solvent gradient was set as follows: 0–5 min, 14% B; 5–5.1 min, 14%–25% B; 5.1–15min, 25% B; 15–17 min, 25%–100% B; 17–18 min, 100% B; 18–18.1 min, 100%–14% B; and 18.1–20 min, 14% B; groups that were added SAP: 0–13 min, 20% B; 13–16 min, 20%–100% B; 16–18 min, 100% B; 18–18.1 min, 100%–20% B; and 18.1–20 min, 20% B.

In the experiment in Section 2.3.4, the solvent gradient was programmed as follows: 0–13 min, 20% B; 13–16 min, 20%–100% B; 16–18 min, 100% B; 18–18.1 min, 100%–20% B; and 18.1–20 min, 20% B.

The solvent gradient in the experiment in Section 2.3.6 was the same as that in Section 2.3.3.

2.8.4. Nano LC-MS/MS analysis

In this experiment, an LTQ-Orbitrap Velos Pro mass spectrometer combined with a nano LC Easy-nLC II LC system (Thermo Fisher Scientific Inc.) was used to collect the proteomics data of the samples.

Samples were injected into a precolumn (Easy-column C_{18}-A1, 100 μm × 20 mm, 5 μm; Thermo Fisher Scientific Inc.), and peptide separation was performed on a reverse-phase C_{18} column (Easy-column C_{18}-A2, 75 μm × 100 mm, 3 μm; Thermo Fisher Scientific Inc.).

Pure water and acetonitrile were used as mobile phase A and phase B, respectively, both containing 0.1% formic acid. The flow rate was 300 nL/min. The solvent gradient was set as follows: 0–70 min, 2%–40% B; 71–75 min, 40%–95% B; and 76–95 min, 95% B. The mass spectrometer parameters were as follows: positive ion mode and data-dependent acquisition mode. The precursor ions were scanned using a MS with Orbitrap with a scan range of *m/z* 350–2000 and resolution of 60,000 (at *m/z* 400). Secondary mass spectrometric analysis was performed on parent ions within the first 15 intensities: collision induced ionization technique with a standardized collision energy of 35 eV.

2.9. Evaluation of SAP-labeling proteins in B. pseudocatenulatum

2.9.1. Extraction of bacterial proteome

B. pseudocatenulatum suspension was inoculated into a GAM liquid medium to activate the bacteria, and the activated bacteria were collected when the OD_{600} value reached 0.8. The bacteria and medium were centrifuged at 6,000 *g* at 4 °C for 15 min. The supernatant was discarded and the precipitate was collected. Bacterial lysis buffer (5 mL) was added to the precipitate and they were mixed equally. The mixed bacterial solutions were subjected to ultrasonic fragmentation for 15 min (ultrasonic fragmentation instrument settings: 400 W; ultrasound 1 s and pause 2 s, for one

Table 1
Mass spectrometry (MS) conditions of the compounds.

Compound	t_R (min)	MRM ion pairs (*m/z*)	Declustering potential (V)	Collision energy (eV)
SA	4.16	861.2/699.1	−90	−15
Rhein	7.28	283.0/239.0	−90	−15
8-Glucosylrheinanthrone	4.01	445.1/283.0	−90	−20
Azomethine derivative of rheinanthrone	7.30	401.1/357.1	−90	−15
Azomethine derivative of 8-glucosylrheinanthrone	3.65	563.2/401.1	−90	−15
1,8-Dihydroxyanthraquinone	8.88	239.0/211.0	−90	−25

t_R: retention time; MRM: multi reaction monitoring; SA: sennoside A.

cycle) in ice-water. Subsequently, the samples were centrifuged at 10,000 *g* for 15 min at 4 °C and the protein supernatant was collected.

2.9.2. Probe labeling proteins

In the experiment to evaluate the labeling efficiency of probe in live bacteria, activated *B. pseudocatenulatum* was cultured in GAM medium containing 50 μM SAP for 30 min.

In the experiment to investigate optimal probe dose, 90 μg of bacterial protein was added to a well of a 96-well plate, and SAP solution was added so that the final concentrations of SAP in the systems were 0, 10, 50, 100, and 250 μM. They were incubated anaerobically, in the dark and with gentle shaking for 30 min at room temperature.

In the experiment to investigate the incubation time of probe and bacterial lysates, 90 μg of bacterial protein was added to a well of a 96-well plate, and SAP solution was added to reach a final concentration of 50 μM. The samples of each group were incubated under anaerobic and dark conditions with gentle shaking for 0 min, 5 min, 15 min, 30 min, and 1 h at room temperature.

All samples in the above groups were irradiated with UV light at 365 nm for 10 min to photo-crosslink the proteins. The bacteria in the activated *B. pseudocatenulatum* solution were collected, added with 1 mL of bacterial lysis buffer, mixed evenly, and subjected to ultrasonic fragmentation in ice water. Then the samples were centrifuged at 10,000 *g* for 15 min at 4 °C and the supernatant was collected. After determination of protein concentration by BCA, all protein concentrations were normalized to 2 mg/mL. To each group of samples, a premixed solution of cyanine5 azide, TCEP, TBTA, and $CuSO_4$ was added for the click chemistry reaction and these mixtures were incubated in the dark at 37 °C for 1 h. The final concentrations of cyanine5 azide, TCEP, TBTA, and $CuSO_4$ were 100 μM, 1 mM, 100 μM, and 1 mM, respectively. Each group of samples was transferred to a 1.5 mL Eppendorf (EP) tube, and loading buffer (5×) was added to the tube. The system was boiled at 95 °C for 5 min. Proteins in each group was separated by 12% SDS-PAGE and visualized using CBB.

2.10. Identifying the protein labeled by SAP

2.10.1. Extraction of bacterial proteome

This part was performed as the experiment in Section 2.9. The concentration of the protein solution was determined using the BCA method, and the bacterial protein concentration was normalized to 2.5 mg/mL.

2.10.2. Probe labeling proteins

To 45 μL of bacterial lysates with a protein concentration of 2.5 mg/mL, SAP solution was added to reach a final concentration of 50 μM. After incubating under anaerobic conditions at room temperature away from light and shaking for 15 min, the samples were irradiated with a 16 W UV lamp at 365 nm for 10 min.

2.10.3. Click chemistry reaction

The samples were added to the premixed solutions of biotin-biotin-polyethylene glycol 3-azide (PEG_3-N_3), TCEP, TBTA, and $CuSO_4$ for click chemistry reaction and incubated in the dark at 37 °C for 1 h. The final concentrations of biotin-PEG_3-N_3, TCEP, TBTA, and $CuSO_4$ in the system were 100 μM, 1 mM, 100 μM, and 1 mM, respectively.

2.10.4. Precipitating proteins

After the reaction, four times the volume of cold acetone was added to ice to precipitate proteins; the proteins were placed at −20 °C for 4 h and centrifuged to obtain the precipitate, and the acetone was volatilized as much as possible. The precipitate was then redissolved in PBS containing 1% SDS.

2.10.5. Prewashing of magnetic beads

Here, 100 μL of streptavidin magnetic bead suspension was vortexed evenly and placed on a magnetic rack for 1 min, and the supernatant was removed. Then, 0.5 mL of washing buffer was added and the resuspended streptavidin magnetic beads were gently aspirated with a pipette gun and placed on a magnetic rack for 30 s. After removing the supernatant, a washing step was completed. Washing was repeated thrice.

2.10.6. Enrichment of probe-labeled proteins using magnetic beads

A protein solution was added to the washed streptavidin magnetic beads. The system was shaken at room temperature for 60 min and placed on a magnetic rack for 1 min. The supernatant was removed.

2.10.7. Bead washing

Here, 1 mL of washing buffer was added to the isolated beads and the beads were resuspended in a centrifuge tube after oscillation. The centrifuge tube was placed on a magnetic frame for 1 min and the supernatant was removed. Washing was repeated 3−4 times.

2.10.8. Protein digestion

There are two common methods used to digest proteins bound to magnetic beads: one is on-bead digestion, which is to add trypsin directly to the “magnetic bead-protein” system to hydrolyze proteins and obtain free peptides; the other is to elute the protein sample from the magnetic beads and then digest it with trypsin to obtain peptides. The “magnetic bead-protein” samples were equally divided and digested using two methods.

1) The disulfide bonds of the protein and alkylation modification of thiols in the protein are generally reduced prior to enzymatic hydrolysis. Here, 200 μL of 50 mM ammonium bicarbonate solution containing 2 mM TCEP was added to the “magnetic bead-protein” sample and the sample was incubated for 10 min at 67 °C to reduce disulfide bonds in the proteins. The sample was cooled to room temperature and the TCEP was removed. Then IAA was added and the sample was treated in the dark for 30 min at room temperature to prevent the reduced free thiols from forming disulfide bonds again, thus alkylating the proteins. IAA was removed and trypsin was added to the sample at a ratio of trypsin: protein of 1:50 (*m*/*m*). After incubation at 4 °C for 1 h, 100 μL of 50 mM ammonium bicarbonate solution was added. The samples were allowed to react overnight at 37 °C and then placed on a magnetic rack for 1 min. The supernatant was collected.
2) A PBS solution containing 0.1% SDS was added to the “magnetic bead-protein” sample, and the sample was heated at 95 °C for 3 min to elute the proteins enriched. The samples were placed on a magnetic rack for 1 min and the supernatant was treated as steps in 1).

The protein eluents were dried under vacuum and prepared for nano LC-MS/MS analysis.

2.10.9. Data analysis of nano LC-MS/MS analysis

The LC-MS/MS raw data were subjected to database search and analysis of the protein sequence database of *B. pseudocatenulatum* in the Universal Protein Resource (UniProt) database using the Sequest HT algorithm in Proteome Discoverer 1.4 software (Thermo Fisher Scientific Inc.). The parameters were set as follows: trypsin,

with a maximum number of missed cleavage sites of 2; IAA alkylation of cysteine as fixed modification; and methionine oxidation as variable modification. The mass error tolerance was set to 10 ppm for the precursor ion scan and 0.8 Da for the secondary fragment ion scan. At the peptide and protein levels, identification was tested with a false positive rate (FDR) of 1%.

2.11. Bioinformatic analysis

Biological function annotation was performed on the proteins labeled by SAP using the Search Tool for Recurring Instances of Neighbouring Genes (STRING) database: protein results were entered into the search box under "multiple proteins" in the STRING database, and the species was selected as "*B. pseudocatenulatum*" to perform the analysis. A protein-protein interaction network diagram, Gene Ontology (GO) enrichment analysis, Kyoto Encyclopedia of Genes and Genomes (KEGG) pathway analysis, and UniProt keywords enrichment information would be obtained.

2.12. Molecular docking of SA and hNQO1/nfrA

2.12.1. SA and hNQO1

Molecular docking was conducted in Molecular Operating Environment (MOE) version 2018.0101. The 2D structure of SA was drawn in ChemBioDraw 2014 and converted to 3D structure in MOE by energy minimization. The 3D structure of the hNQO1 protein was downloaded from the RCSB Protein Data Bank (PDB) (PDB ID: 2F1O). Before docking, the force field of Assisted Model Building and Energy Refinement (AMBER)10: Extended Hückel Theory (EHT) and the implicit solvation model of the Reaction Field (R-field) were selected. MOE-Dock was used for molecular docking simulations of SA with hNQO1. The docking workflow followed the "induced fit" protocol, in which the side chains of the receptor pocket were allowed to move according to the ligand conformations, with a constraint on their positions. The weight used for tethering side chain atoms to their original positions was 10. For each ligand, all docked poses of which were ranked by London dG scoring first, then a force field refinement was performed on the top 20 poses followed by a rescoring of GBVI/WSA dG. Molecular graphics were generated using PyMOL (version REF).

2.12.2. SA and nfrA

The molecular structure of SA was drawn using ChemDraw and energy optimization was performed using Chem3D. We entered the UniProt database, obtained the amino acid sequence of nfrA, constructed a 3D model of the protein based on AlphaFold 2, and acquired a protein receptor structure file. AutoDock was used to evaluate the binding activity of SA to the target protein.

2.13. Recombinant expression of nfrA

2.13.1. Construction of the expression vector

Gene synthesis was performed using the target gene sequence (GenBank: CUO08416.1) provided in the National Center for Biotechnology Information (NCBI) database, and the expression vector was constructed. This part was completed by Beijing Huada Protein Research and Development Center Co., Ltd. (Beijing, China).

2.13.2. Plate coating

Competent cells stored at −80 °C were taken out and placed on ice for slow thawing. Competent cells were added to the junction products of *nfrA* and pET-32a (+) vector, mixed evenly, placed on ice for 30 min, and subjected to heat shock at 42 °C for 90 s. After an ice bath for 2 min, 800 μL of nonresistant LB medium was added and cultured at 37 °C for 45 min. The cultures were centrifuged at 5000 rpm for 3 min to obtain bacterial cells. The bacteria were resuspended, coated on LB solid medium containing kanamycin, and incubated upside down at 37 °C overnight.

2.13.3. Protein expression

Bacteria were inoculated into LB liquid medium containing kanamycin and cultured at 37 °C overnight with shaking. The cultured medium was transferred to 250 mL of LB liquid medium containing kanamycin in a ratio of 1:50 (*m*/*m*) and shaken at 200 rpm at 37 °C to an OD_{600} value of 0.6–0.8, and IPTG (final concentration of 0.5 mM) was added for induction overnight at 16 °C.

The cells were centrifuged at 8000 rpm for 6 min at 4 °C. The supernatant was discarded and the cells were collected, washed with 20–30 mL of 10 mM Tris-HCl (pH 8.0) solution and sonicated in an ice bath (500 W, 180 times, 5 s each time with an interval of 5 s). Finally, the expressed protein was detected by SDS-PAGE.

2.13.4. Purification of proteins

A nickel column (Ni Sepharose 6 Fast Flow; GE Healthcare, Marlborough, MA, USA) was cleaned with deionized water to pH 7.0. Nickel was attached to the column until its pH value was 2–3. The column was washed with deionized water to pH 7.0 and balanced with 100 mL of 10 mM Tris-HCl (pH 8.0) and 50 mL of a 10 mM solution of Tris-HCl (pH 8.0, containing 0.5 M sodium chloride) successively.

The recombinant protein solution was added to the nickel column, and the column was washed with 10 mM Tris-HCl (pH 8.0, containing 0.5 M sodium chloride) to remove foreign proteins. After eluting the column with 10 mM Tris-HCl (pH 8.0, containing 0.5 M sodium chloride) containing 15, 60, and 300 mM imidazole in succession, the eluents were collected. The effect of protein purification was detected by SDS-PAGE. Finally, the protein was desalted and concentrated in a Millipore ultrafiltration tube (Billerica, MA, USA) for subsequent verification of enzymatic function.

2.14. Surface plasmon resonance (SPR) analysis

The biomolecular interaction between SA and nfrA was analyzed by SPR using a Biacore 8k system. After activation with *N*-hydroxysulfosuccinimide, the carboxymethylated 5 sensor chip was linked to the recombinant nfrA protein, which was diluted to a concentration of 40 μg/mL using acetic acid (pH 4.0), followed by blocking with ethanolamine. Gradient concentrations of SA were injected at a flow rate of 30 μL/min in running buffer (0.05% (*V*/*V*) Tween 20 and 5% (*V*/*V*) DMSO in PBS). The SPR test was then performed, and the results were analyzed using Biacore evaluation software.

2.15. Statistical analysis

Statistical analyses were conducted using Student's *t*-test between two groups using GraphPad Prism version 5 (GraphPad Software Inc., San Diego, CA, USA). Data were expressed as mean ± standard deviation (SD), and *P* values less than 0.05 were considered to be statistically significant.

3. Results

3.1. Effect of common reductants on the reduction of SA in vitro

As well known, some reduction reactions *in vivo* are mediated by common reductants [34–37]. Therefore, we first investigated the effect of common reductants on the reduction of SA *in vitro* by MS. As shown in Fig. S1, the peaks of the azomethine derivatives of rheinanthrone and 8-glucosylrheinanthrone were hard to be

observed in an *in vitro* experiment including glutathione, NADH, ascorbic acid, DTT, and L-cysteine.

3.2. Screening active strains reducing SA to rheinanthrone

Previous studies display that gut bacteria are key mediators in the transformation of SA to rheinanthrone [23]. Choosing appropriate active strains that are capable of metabolizing SA is crucial for the identification of SA reductases. On the basis of the literature research, we found that 20 reported strains can metabolize sennoside A/B (SA/B) or sennidin A/B. Given the potential of bacteria dominating in the gut microbiota to influence the metabolism of drugs to a significant degree and the priority of probiotics for effective transformation of SA, a total of nine strains were selected for further screening [38–42]. The nine strains were incubated with SA under anaerobic conditions, and reductive metabolites (rheinanthrone and 8-glucosylrheinanthrone) were determined as the azomethine derivatives by adding *N*,*N*′-dimethy-4-nitrosoaniline as described in the previous paper [23] using UPLC-Q-TOF/MS (Fig. 1A). The azomethine derivatives of rheinanthrone and 8-glucosylrheinanthrone were detected in the incubation systems of *B. pseudocatenulatum* (Figs. 1B and C) and *Bifidobacterium breve* (Fig. S2). Only the azomethine derivatives of 8-glucosylrheinanthrone could be detected in the incubation systems of *Clostridium butyricum* and *Clostridium perfringens* (Fig. S2). The results demonstrated that the four strains were capable of reducing SA. Among them, *B. pseudocatenulatum* is one of the predominant intestinal bacterial strains. Thus, we took it as a model strain for subsequent studies.

3.3. Design, synthesis, and characterization of photoaffinity active SAP

To identify SA reductases in *B. pseudocatenulatum*, we designed SAP, which is composed of three parts: a recognition group (SA scaffold), a bioorthogonal group (alkyl handle), and a photoreactive group (diazirine). The SA scaffold facilitates the close proximity of SAP to targeted proteins, thereby promoting selective binding. The diazirine group is activated to form carbene intermediates to bind proximal proteins of interest covalently under UV irradiation. The alkyne handle is used to visualize and enrich interactional proteins by azide-containing biotin or fluorescein via the copper-catalyzed azide-alkyne cycloaddition (CuAAC) reaction. To synthesize SAP, SA was bound with 2-(3-(but-3-yn-1-yl)-3*H*-diazirin-3-yl)ethan-1-amine containing both diaziridine and alkynyl through an amidation reaction. The resulting products were purified by flash chromatography, yielding dark brown solids with a productivity of 23.2%. The purified products were characterized through NMR and MS (Fig. S3). The results demonstrated that the alkynyl and diaziridine moieties had modified the SA scaffold.

3.4. Investigation on the activity of photoaffinity active probe

In the construction of SAP, the carboxyl group of SA was chemically modified. To ascertain whether SAP retained its activity to be catalyzed by SA reductases, a model enzyme was selected to investigate the activity of SAP as a substrate of SA reductase and its ability to label proteins.

To find the model enzyme, we first analyzed the possible types of SA reductases. Previous studies have indicated that the reductase of SA may be an NADH-flavin reductase. More importantly, SA is a kind of dianthrone that contains a quinone backbone. As one of the NADH-flavin reductases, NQO is a common oxidoreductase family in bacteria, playing an essential role in the respiration and metabolism of bacteria [43–46]. Therefore, we speculate that NQO in gut microbiota can reduce SA. To validate our hypothesis, different concentrations of the NQO inhibitor DIC were added to the incubation system of single strains or human gut microbiota suspension with SA. The results showed that the content of 8-glucosylrheinanthrone in four strains, except for *Clostridium perfringens*, significantly decreased with an increase in DIC concentration (Figs. S4A and B). In the incubation system of human gut microbiota suspension, with an increase in DIC concentration, the contents of rheinanthrone and 8-glucosylrheinanthrone also tended to decrease (Fig. S4C). We subsequently treated mice with the NQO inducer BHA and the inhibitor DIC, and then, the mice were orally administered with SA. Fecal samples were collected to determine the activity of NQO in the gut microbiota (Fig. S4D). Meanwhile, we evaluated the purgative effect of the treatment by testing total stool grains, loose stool grade, loose stool rate, and diarrhea index. These results suggested that BHA increased the NQO activity in the gut microbiota of mice and improved the purgative effect of SA, and DIC had an opposite effect (Figs. S4E–H). The aforementioned results further indicated that NQO was an essential enzyme involved in the reductive metabolism of SA and was positively correlated with its purgative activity.

As the crystal structures of hNQO1 have been illustrated and are available in the PDB, we performed a computer-assisted docking analysis of hNQO1 and SA. The two structures exhibited excellent docking performance when SA docked onto hNQO1 with a binding free energy of −9.87 kcal/mol. The binding mode of hNQO1 with SA is illustrated in Figs. 2A and B. The analysis of the binding mode of SA to hNQO1 revealed the interaction with conserved active site residues of the enzyme. These results show that hNQO1 could combine SA. Subsequently, the recombinantly expressed hNQO1 was incubated with SA. With time, the yield of metabolite 8-glucosylrheinanthrone increased to a maximum at 1 h and then gradually decreased (Fig. 2C). This is inconsistent with our expected results. Considering that the 8-glucosylrheinanthrone is susceptible to oxidation, we subsequently detected its oxidative product, rhein-8-*O*-β-D-glucoside, and found that the content of rhein-8-*O*-β-D-glucoside gradually increased with time, indicating that 8-glucosylrheinanthrone was almost completely converted to its oxidized form in the later stage (Fig. 2D). In addition, the relative total amount of the two metabolites gradually increased with time, and reached the highest value at 6 h (Fig. 2E). To further prove that hNQO1 could reduce SA, we investigated whether the reductive metabolism of SA could be inhibited by adding the inhibitor DIC to the incubation system of hNQO1 and SA. As shown in Figs. 2F and G, compared with the control group without DIC, the addition of DIC significantly inhibited the consumption of SA and the production of reducing metabolites from SA. The above results indicated that hNQO1 could reduce SA, which could be used as a model enzyme to evaluate whether SAP retains the activity of SA.

Similar to the results of SA, the anaerobic incubation of hNQO1 and SAP at 37 °C revealed the presence of derivatives of SAP metabolites in the system, and no such products were detected in the control group without hNQO1, either at 0.5 or 12 h (Figs. 3A–C).

To ascertain the ability of SAP to label proteins covalently, a model protein OVA was used. The probe-labeled proteins were conjugated with cyanine5 azide via CuAAC, separated by SDS-PAGE and visualized using fluorescence signals and CBB analysis (Fig. 3D). As shown in Fig. 3E, the CBB of each lane exhibited a near-uniform pattern, suggesting that the protein content of each lane was largely consistent, thereby negating the potential influence of protein quantity on the observed differences in fluorescence signals. The fluorescence signal was different in each lane. Upon coincubation of SAP and OVA prior to UV irradiation, the OVA lane (lane 5) exhibited a stronger fluorescence signal compared with that of the group without undergoing UV exposure (lane 4) and that

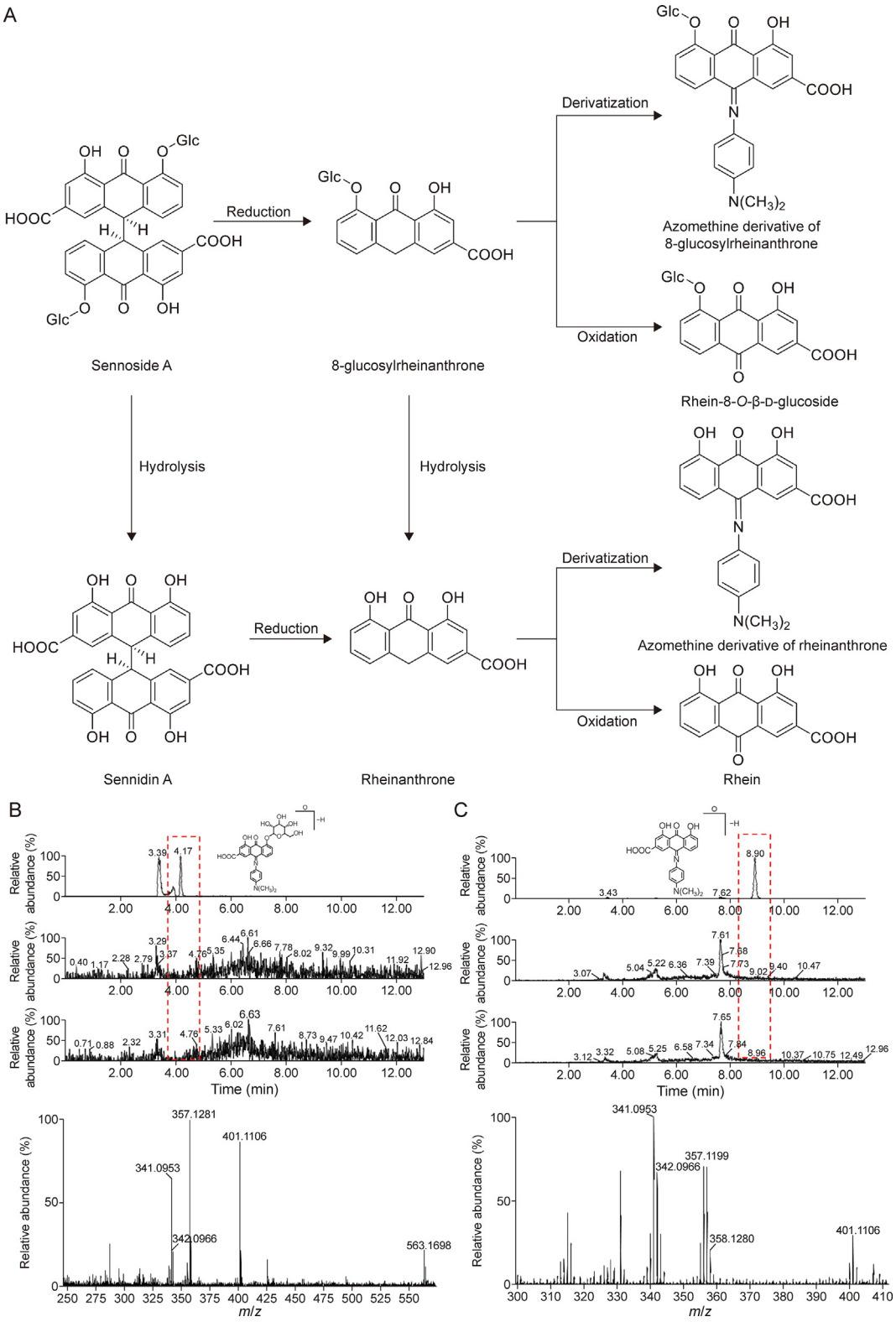

Fig. 1. *Bifidobacterium pseudocatenulatum* (*B. pseudocatenulatum*) could reduce sennoside A (SA). (A) Metabolic pathways of SA in bacterial strains and the derivatization of reductive products. (B, C) Liquid chromatography-tandem mass spectrometry (LC-MS/MS) analysis of azomethyl derivatives of 8-glucosylrheinanthrone (B) and rheinanthrone (C).

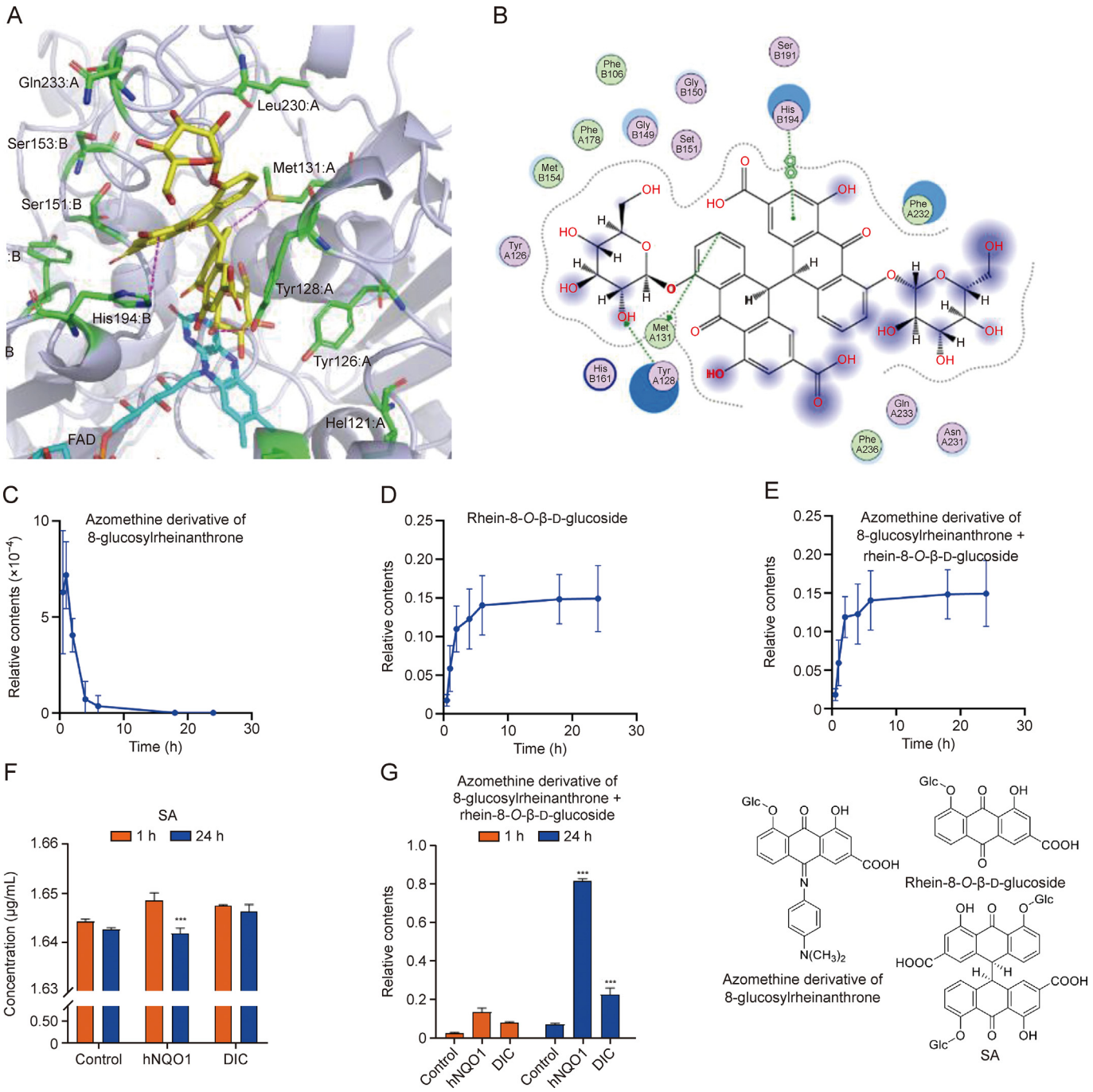

Fig. 2. Activity of human nicotinamide adenine dinucleotide (phosphate) (NAD(P)H): quinone dehydrogenase 1 (hNQO1) to reduce sennoside A (SA) was verified. (A, B) The three-dimensional (3D) (A) and 2D (B) binding mode of hNQO1 and SA. (C–E) The production of 8-glucosylrheinanthrone (C), rhein-8-*O*-β-D-glucoside (D), and total metabolites of SA (E) changed over time after incubating hNQO1 with SA. (F, G) The amounts of residual SA (F) and the reductive products (G) after incubating hNQO1 with SA and dicoumarol (DIC). $^{***}P < 0.001$, compared with the control group. FAD: flavin adenine dinucleotide.

of the group without introducing cyanine5 azide in the same position. The lack of signal in the same position on lane 1 indicates that the fluorescent signal was free from the influence of UV irradiation and fluorescein labeling.

3.5. Identifying potential SA reductases based on SAP

To label SA reductases in live strains, *B. pseudocatenulatum* was incubated with SAP, after which SDS-PAGE and in-gel fluorescence analysis were performed. The results showed poor labeling, which is probably due to the large molecular weight of SAP and its limited capacity to permeate the bacterial cell membrane (Fig. 4A). To promote the labeling efficiency of SAP, lysates of *B. pseudocatenulatum* were used. It was observed that the fluorescence signal was significantly enhanced (Fig. 4A). The results indicated that SAP could label bacterial proteins efficiently. To determine optimal experimental conditions for the subsequent identification of SA reductases, the incubation time and dose of SAP were further optimized through observing fluorescence signals in experiments with a series of incubation times and doses of SAP. It was shown that the lanes displayed more extensive fluorescence signals with 50 μM SAP for 15 min, indicating a superior labeling effect (Figs. 4B and C).

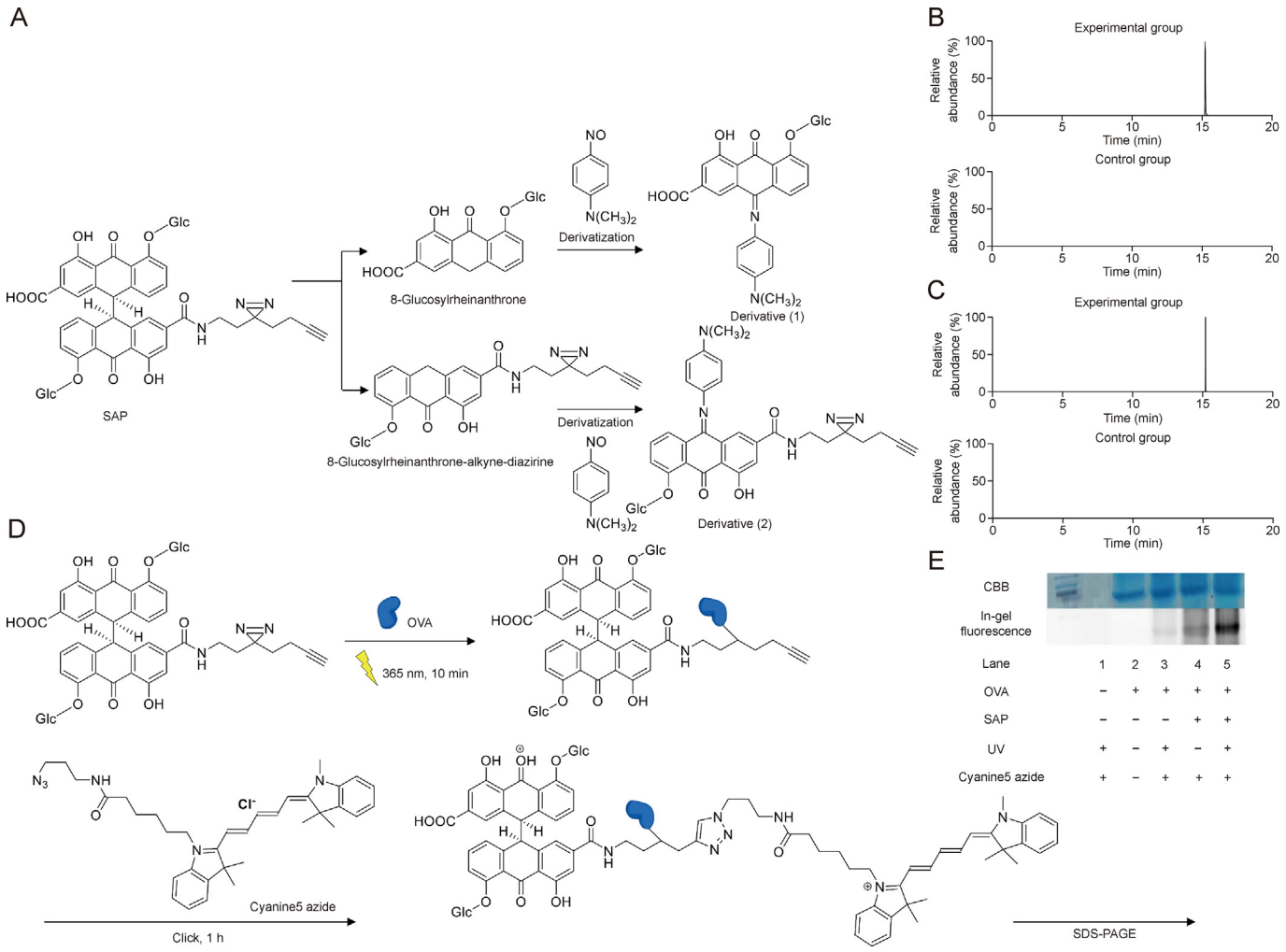

Fig. 3. The photoaffinity probe based on sennoside A (SA) (SAP) could be reduced by human nicotinamide adenine dinucleotide (phosphate) (NAD(P)H) quinone dehydrogenase 1 (hNQO1) and label proteins under ultraviolet (UV) irradiation. (A) Two inferred reductive products of SAP and derivatives of the products. (B, C) Liquid chromatography-tandem mass spectrometry (LC-MS/MS) analysis of the reductive products of SAP catalyzed by hNQO1 at 0.5 (B) and 12 h (C) (experimental group I and control group II). (D) Workflow of in-gel fluorescence analysis. (E) Evaluation of labeling effects of SAP by in-gel fluorescence. OVA: ovalbumin; CBB: Coomassie brilliant blue; SDS-PAGE: sodium dodecyl sulfate-polyacrylamide gel electrophoresis.

To identify SA reductases with SAP, lysates of *B. pseudocatenulatum* were incubated with 50 μM SAP for 15 min. The system was then exposed to UV irradiation for inducing photo-crosslinking. The alkynyl handle of SAP was linked with azido modified biotin by CuAAC reactions. The labeled proteins were enriched by streptavidin magnetic beads via a specific interaction between biotin and streptavidin. Subsequently, the enriched proteins were identified by MS. Two different digestion methods were used (Fig. 4D). The two methods varied in the operation procedure. In one method, tryptic digestion was performed after proteins were eluted from beads at 95 °C for 3 min. The other method, on-bead digestion, performed tryptic digestion in the protein-bead sample. It was demonstrated that 309 proteins were identified using the former method (Tables S1 and S2) [47] and 287 proteins were identified using the latter method (Tables S3 and S4). The two methods exhibited an overlap of 199 proteins (Fig. 4E). To excavate SA reductases more comprehensively, we merged proteins from the two methods (397 proteins) for later analysis.

3.6. Screening SA reductases

To obtain annotated information on the proteins identified from lysates of *B. pseudocatenulatum*, bioinformatic analysis was applied to the proteins using the STRING database. This included GO and KEGG pathway analyses. The results are shown in Fig. 5A. GO analysis comprises three sections: molecular function (MF), biological process (BP), and cellular component (CC). GO BP analysis showed that the labeled proteins were mainly involved in metabolism, organic matter metabolism, nitrogen compound metabolism, oxidation-reduction, and other processes. GO MF analysis revealed that the most prevalent items were those related to heterocyclic compounds and organic ring compounds. GO CC analysis revealed that the majority of the labeled proteins were located in ribosomes, nonmembranous organelles, and the cytoplasm. Profiling pathways contributes to a further understanding of the biological functions of genes. KEGG pathway analysis revealed that functionally enriched pathways included metabolism, secondary metabolite biosynthesis, ribosomes, and microbial metabolic pathways in different environments. UniProt keywords showed the annotation information of proteins, and the keywords mainly were cytoplasm, ribosomal RNA (rRNA) binding, magnesium, oxidoreductase, NADP, and so forth. It indicated that SA reductase may be an oxidoreductase, may be located in the cytoplasm, and may work with NADP. Interestingly, excluding general and broad enrichment items in the GO BP analysis, the metabolism of nitrogenous compounds occupied large proportions of

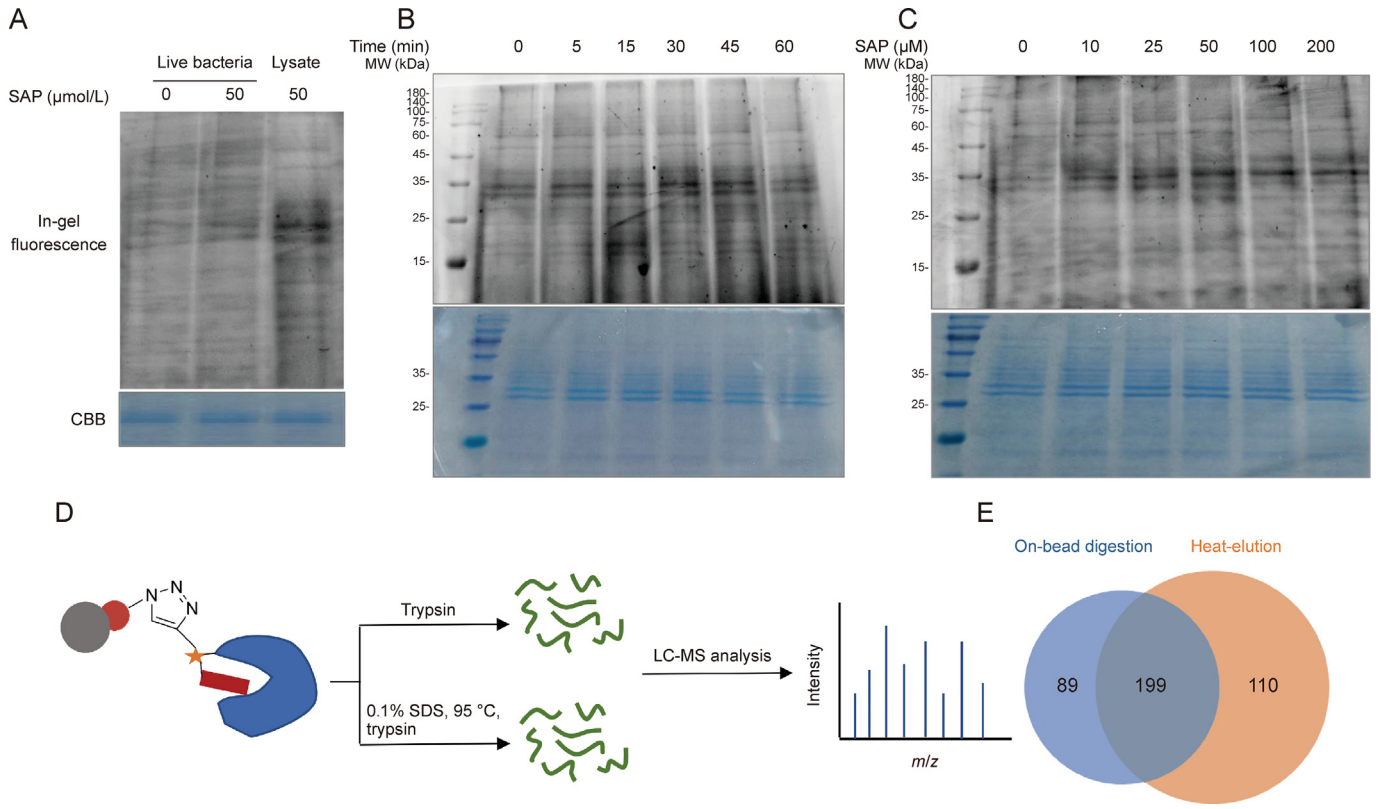

Fig. 4. The potent sennoside A (SA) reductases in *Bifidobacterium pseudocatenulatum* (*B. pseudocatenulatum*) were labeled by the photoaffinity probe based on SA (SAP). (A) Labeling of live bacterial cells or bacterial lysates with SAP. (B) Labeling of bacterial lysates with SAP under a series of incubation time. (C) Labeling of bacterial lysates with a series of dose of SAP. (D, E) Two digestion procedures for proteins enriched (D) and Venn diagram analysis of the corresponding results (E). CBB: Coomassie brilliant blue; MW: molecular weight; SDS: sodium dodecyl sulfate; LC-MS: liquid chromatography-mass spectrometry.

enrichment items. It prompted that SA reductases are probably involved in the metabolism of nitrogen compounds.

To narrow the scope of candidates for SA reductases, we queried the UniProt database and literature to select proteins that can catalyze reductive reactions for further analysis. This yielded 17 proteins from 397 proteins (Table S5). Interestingly, when optimizing the incubating time of SAP and lysates of *B. pseudocatenulatum*, it was observed that SAP could efficiently label low abundance proteins with a molecular weight between 25 and 35 kDa (Fig. 4C). This phenomenon indicated that proteins with a molecular weight between 25 and 35 kDa were highly probable to be SA reductases. Thereafter, the molecular weights of the 17 proteins related to the reduction reaction were queried, and it was found that nfrA [48] had a molecular weight of 28,661 Da. In addition, nfrA was identified in two protein samples using two digestion methods. The results support nfrA as a SA reductase.

NfrA belongs to the flavin oxidoreductase/NADH oxidase family that could catalyze the reduction of nitrogen compounds, quinone compounds, or flavin compounds by transferring double electrons with NAD(P)H as an electron donor and FMN/flavin adenine dinucleotide (FAD) as an electron carrier. The addition of DIC, a NQO and nitroreductase inhibitor [49,50], to incubation systems of *B. pseudocatenulatum* and SA resulted in the inhibition of the reductive products of SA in a concentration-dependent manner (Figs. S4A and B). The results indicated that the proteins of the flavin oxidoreductase/NADH oxidase family are potential SA reductases in *B. pseudocatenulatum* and therefore supported nfrA to be a potent SA reductase.

3.7. Validating activity of nfrA to reduce SA

To validate the activity of nfrA to reduce SA, we first verified whether the potential target metabolic enzyme (nfrA) interacted with SA by molecular docking. A 3D model of nfrA was constructed based on AlphaFold 2 [51] to acquire structural information of protein receptors. The optimal molecular docking result was acquired via AutoDock operation analysis (Fig. 5B). The binding energy was −8.1 kcal/mol, indicating a strong binding affinity between nfrA and SA. SA could form six hydrogen bonds with residues Asp176, Arg17, Ala8, Thr12, Glu15, and Pro173 in the binding pocket of nfrA and hydrophobic bonds with several other residues (Fig. 5C). These hydrogen bonds and hydrophobic bonds probably support nfrA to recognize and bind SA.

The results of molecular docking increased our confidence. Therefore, *E. coli* was used to recombine and express the nfrA protein, which was purified through a nickel-affinity chromatography column to further verify the activity of nfrA in reducing SA. The purified recombinant nfrA was then incubated with SA at 37 °C in an anaerobic environment. Products were taken at various incubation time intervals (0.5, 1, and 4 h) to quantify derivatives of reductive products (8-glucosylrheinanthrone) or oxidation products (rhein-8-*O*-β-D-glucoside) of SA. A negative control without nfrA was performed as the same procedure. As shown in Figs. 5D and E, the concentration of the reductive products and oxidation products exhibited a notable increase from 0.5 to 4 h in the experimental group. In the control group, the former remained at a low and relatively constant level throughout the experiment and the latter increased significantly from 0.5 to 1 h and then remained at a similar

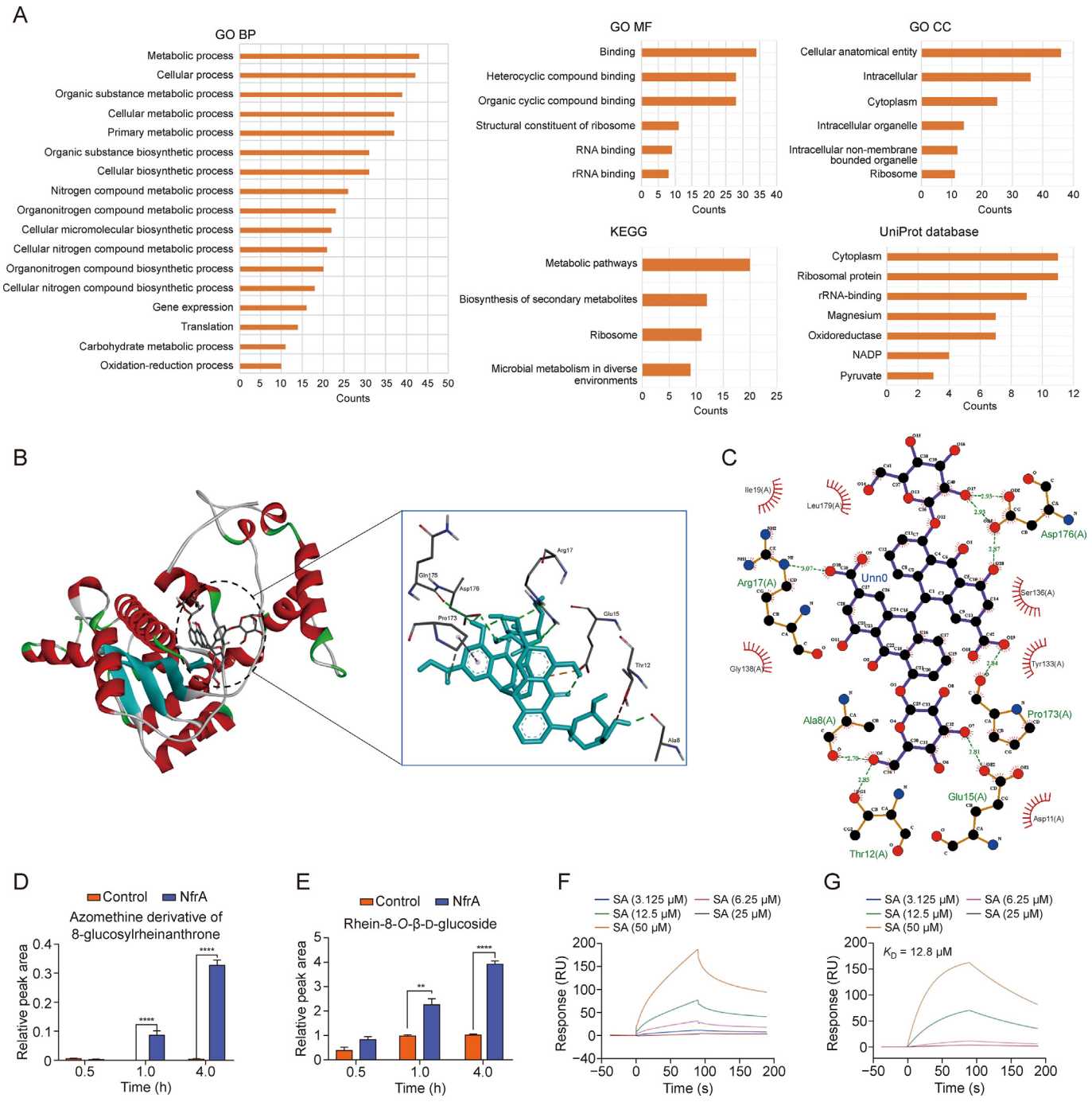

Fig. 5. Chromate reductase/nicotinamide adenine dinucleotide (NADH) phosphate (NADPH)-dependent flavin mononucleotide (FMN) reductase/oxygen-insensitive NADPH nitroreductase (nfrA) was selected from the identified proteins and validated as a sennoside A (SA) reductase. (A) Bioinformatic analysis of 397 proteins labeled by the photoaffinity probe based on SA (SAP). (B, C) The three-dimensional (3D) (B) and 2D binding mode (C) of nfrA and SA. (D, E) The amount of azomethine derivatives of 8-glucosylrheinanthrone (D) and rhein-8-*O*-β-D-glucoside (E) changed over time in the control and nfrA experimental groups. $^{**}P < 0.01$ and $^{****}P < 0.0001$, compared with the control group. (F, G) Kinetic interaction between SA and nfrA (F) was performed using surface plasmon resonance (SPR) analysis. The fitted curves were mapped for different concentrations of SA (G) binding to nfrA using kinetic analysis. GO BP: Gene Ontology (GO) biological process; GO MF: GO molecular function; rRNA: ribosomal RNA; GO CC: GO cellular component; KEGG: Kyoto Encyclopedia of Genes and Genomes; NADP: nicotinamide adenine dinucleotide phosphate.

level from 1 to 4 h. Notably, the contents of the two products were significantly higher in the experimental group than in the control group at 1 and 4 h, and the two groups exhibited nearly consistent concentrations at 0.5 h. These findings provide quantitative evidence that nfrA can reduce SA and that it functions as a SA reductase in *B. pseudocatenulatum*. Their binding affinity was also measured using SPR analysis, which determined a binding constant (K_D) of 12.8 μM, indicating a strong interaction between SA and nfrA (Figs. 5F and G).

4. Discussion

Methods excavating unknown enzymes include genomics analysis, transcriptomics analysis, proteomics analysis, and mining based on known enzymes. The former three methods offer limited insights into enzyme activity under specific conditions. The lack of conserved amino acid residues in reductases presents a challenge to the identification of SA reductases through mining based on known enzymes,

as SA reductases remain undiscovered. ABPP uses tailor-made ABPs to covalently label specific amino acid residues in the binding pocket of the enzymes [15,16]. However, the lack of conserved amino acid residues in reductases make the synthesis of a probe binding covalently with target reductases in gut bacteria challenging [18]. Considering that a photoreactive group could transform to a highly active intermediate to interact with the pocket of enzymes [19,20], diazirine was incorporated to design SAP for identifying reductases involved in the transformation of SA to rheinanthrone. Using SAP and MS-based chemoproteomics, we identified one SA reductase in *B. pseudocatenulatum*, i.e., nfrA.

Before performing ABPP on bacterial proteins, the influence of common reductants *in vitro* on the reduction of SA was ruled out (Fig. S1). Not all gut bacteria participate in the reduction of SA, so appropriate active strains were selected [23]. Thus, *B. pseudocatenulatum* was selected for further study, which is consistent with the result of Matsumoto et al. [39].

An appropriate probe is crucial to perform ABPP. A model enzyme hNQO1 was used to ascertain that SAP could be catalyzed by SA reductases (Figs. 3A–C). Gel-based analysis was applied to ascertain the ability of SAP to label SA reductases covalently. On the basis of the consistent CBB staining of each lane (Fig. 3E), a stronger fluorescence signal represents a higher labeling efficiency of SAP. The labeling efficiency of SAP was significantly reduced without UV irradiation. This indicated that the diazirine group of SAP interacted with the enzyme in a UV dependent manner. The diminished fluorescence signal of the group without adding SAP (lane 3) further ruled out the possibility of nonspecific binding of cyanine5 azide to OVA.

In situ labeling has a promising application in microbiology, but a poorer labeling than that of SAP-labeling bacterial lysates was observed. To excavate potential SA reductases more efficiently, lysates were used for protein identification using MS, which has emerged as the preferred method for in-depth characterization of the protein components. The quantities of identified proteins differed when two digestion methods were used. One method was on-bead digestion [47]. In the other method, tryptic digestion was performed after proteins were eluted at 95 °C [32] for 3 min (Fig. 4D). The latter method is based on the combined action of SDS and heat to break the interaction between streptavidin and biotin, which may result in several proteins not being eluted. The former method does not involve the elution process, but peptides labeled by SAP are hard to be eluted, which changed the quantity of identified proteins. Thus, the two methods show many specific proteins (Fig. 4E). By integrating data from two digestion methods, a total of 397 proteins were identified in *B. pseudocatenulatum*. A combination of bioinformatic analysis, UniProt database research, and literature research further narrowed the range to 17 proteins. Inspired by the observation that low-abundance proteins with a molecular weight between 25 and 35 kDa exhibited significant fluorescence signals upon in-gel analysis, we inferred that nfrA, a protein with a molecular weight of 28,661 Da, was a SA reductase. Molecular docking research and SPR analysis showed a strong interaction between nfrA and SA. The MS-based quantitative analysis of the incubation system of recombinant nfrA with SA further validated that nfrA is a SA reductase. Future experiments will focus on understanding the catalytic mechanism of nfrA reducing SA.

5. Conclusion

SAP was synthesized and applied innovatively to probe SA reductases in gut bacteria. The SA scaffold enables SAP to target and approach SA reductases, and the diazirine group of SAP labels adjacent SA reductases covalently by forming carbene intermediates that react with C–H bonds in the binding pocket under UV irradiation. In the research, we ruled out the influences of reductants on the reducing metabolism of SA. Combined with MS-based chemoproteomics, we identified nfrA as a SA reductase in *B. pseudocatenulatum* and further validated its catalytic activity by incubating recombinant nfrA with SAP. Our study fulfills the discovery and identification of metabolic reductases in gut bacteria and contributes to illuminating the mechanism of SA to exert lapactic effects. Our work offers a fresh reference to annotate reductases encoded by the microbiome in the human intestinal tract and a novel perspective on elucidating the interactive mechanisms between gut bacteria and SA.

CRediT authorship contribution statement

Yang Xu: Writing – review & editing, Writing – original draft, Investigation. **Shujing Lv:** Writing – review & editing, Writing – original draft, Investigation. **Xiang Li:** Writing – review & editing, Writing – original draft, Formal analysis. **Chuanjia Zhai:** Writing – review & editing, Formal analysis. **Yulian Shi:** Writing – review & editing, Formal analysis. **Xuejiao Li:** Writing – review & editing, Formal analysis. **Zhiyang Feng:** Writing – review & editing, Formal analysis. **Gan Luo:** Writing – review & editing, Formal analysis. **Ying Wang:** Writing – review & editing, Methodology, Conceptualization. **Xiaoyan Gao:** Writing – review & editing, Methodology, Funding acquisition, Conceptualization.

Declaration of competing interest

The authors declare that there are no conflicts of interest.

Acknowledgments

This work was supported by the National Natural Science Foundation of China (Grant Nos.: U21A20407 and 81973467) and Beijing Natural Science Foundation, China (Grant No.: 7222276).

Appendix A. Supplementary data

Supplementary data to this article can be found online at https://doi.org/10.1016/j.jpha.2024.101108.

References

[1] N. Koppel, J.E. Bisanz, M.E. Pandelia, et al., Discovery and characterization of a prevalent human gut bacterial enzyme sufficient for the inactivation of a family of plant toxins, Elife 7 (2018), e33953.
[2] A. Basit, J.K. Amory, V.S. Mettu, et al., Relevance of human aldoketoreductases and microbial β-glucuronidases in testosterone disposition, Drug Metab. Dispos. 51 (2023) 427–435.
[3] H.-C. Lan, S.-Z. Li, K. Li, et al., *In vitro* human intestinal microbiota biotransformation of nobiletin using liquid chromatography-mass spectrometry analysis and background subtraction strategy, J. Sep. Sci. 44 (2021) 2046–2053.
[4] F. Guarner, J.R. Malagelada, Gut flora in health and disease, Lancet 361 (2003) 512–519.
[5] J. Qin, R. Li, J. Raes, et al., A human gut microbial gene catalogue established by metagenomic sequencing, Nature 464 (2010) 59–65.
[6] L. Qian, H. Ouyang, L. Gordils-Valentin, et al., Identification of gut bacterial enzymes for keto-reductive metabolism of xenobiotics, ACS Chem. Biol. 17 (2022) 1665–1671.
[7] V. Maini Rekdal, E.N. Bess, J.E. Bisanz, et al., Discovery and inhibition of an interspecies gut bacterial pathway for Levodopa metabolism, Science 364 (2019), eaau6323.
[8] K.C. Mok, O.M. Sokolovskaya, A.M. Nicolas, et al., Identification of a novel cobamide remodeling enzyme in the beneficial human gut bacterium *Akkermansia muciniphila*, mBio 11 (2020) e02507–e02520.
[9] G. Yang, S. Hong, P. Yang, et al., Discovery of an ene-reductase for initiating flavone and flavonol catabolism in gut bacteria, Nat. Commun. 12 (2021), 790.
[10] L. Shao, L. Wang, Y.-Y. Shi, et al., Biotransformation of the saponins in *Panax notoginseng* leaves mediated by gut microbiota from insomniac patients, J. Sep. Sci. 46 (2023), e2200803.
[11] H.J. Haiser, D.B. Gootenberg, K. Chatman, et al., Predicting and manipulating cardiac drug inactivation by the human gut bacterium Eggerthella lenta, Science 341 (2013) 295–298.

[12] S.C. Peck, K. Denger, A. Burrichter, et al., A glycyl radical enzyme enables hydrogen sulfide production by the human intestinal bacterium *Bilophila wadsworthia*, Proc. Natl. Acad. Sci. U S A 116 (2019) 3171–3176.
[13] C. Lemay-St-Denis, L. Alejaldre, Z. Jemouai, et al., A conserved SH3-like fold in diverse putative proteins tetramerizes into an oxidoreductase providing an antimicrobial resistance phenotype, Philos. Trans. R. Soc. Lond. B Biol. Sci. 378 (2023), 20220040.
[14] Q. Jin, J. Wu, Y. Wu, et al., Optical substrates for drug-metabolizing enzymes: Recent advances and future perspectives, Acta Pharm. Sin. B 12 (2022) 1068–1099.
[15] H.Y. Nam, D. Song, J. Eo, et al., Activity-based probes for the high temperature requirement A serine proteases, ACS Chem. Biol. 15 (2020) 2346–2354.
[16] H.S. Hahm, E.K. Toroitich, A.L. Borne, et al., Global targeting of functional tyrosines using sulfur-triazole exchange chemistry, Nat. Chem. Biol. 16 (2020) 150–159.
[17] Y. Liu, M.P. Patricelli, B.F. Cravatt, Activity-based protein profiling: The serine hydrolases, Proc. Natl. Acad. Sci. U S A 96 (1999) 14694–14699.
[18] R. Fuerst, R. Breinbauer, Activity-based protein profiling (ABPP) of oxidoreductases, Chembiochem 22 (2021) 630–638.
[19] F. Xiao, X. Zhang, X. Lei, Recent developments and applications of photoconjugation chemistry, Chimia (Aarau) 72 (2018) 782–790.
[20] U. Seneviratne, Z. Huang, C.W. Am Ende, et al., Photoaffinity labeling and quantitative chemical proteomics identify LXRβ as the functional target of enhancers of astrocytic apoE, Cell Chem. Biol. 28 (2021) 148–157.e7.
[21] Y. Zhou, W. Li, W. You, et al., Discovery of *Arabidopsis* UGT73C1 as a steviol-catalyzing UDP-glycosyltransferase with chemical probes, Chem. Commun. 54 (2018) 7179–7182.
[22] K. Sasaki, K. Yamauchi, S. Kuwano, Metabolic activation of sennoside A in mice, Planta Med. 37 (1979) 370–378.
[23] K. Kobashi, T. Nishimura, M. Kusaka, et al., Metabolism of sennosides by human intestinal bacteria, Planta Med. 40 (1980) 225–236.
[24] J. Le, H. Ji, X. Zhou, et al., Pharmacology, toxicology, and metabolism of sennoside A, A medicinal plant-derived natural compound, Front Pharmacol. 12 (2021), 714586.
[25] L. Yang, T. Akao, K. Kobashi, et al., Purification and characterization of a novel sennoside-hydrolyzing beta-glucosidase from *Bifidobacterium* sp. strain SEN, a human intestinal anaerobe, Biol. Pharm. Bull. 19 (1996) 705–709.
[26] T. Akao, Q.M. Che, K. Kobashi, et al., Isolation of a human intestinal anaerobe, *Bifidobacterium sp.* strain SEN, capable of hydrolyzing sennosides to sennidins, Appl. Environ. Microbiol. 60 (1994) 1041–1043.
[27] L. Yang, T. Akao, K. Kobashi, et al., A sennoside-hydrolyzing beta-glucosidase from *Bifidobacterium sp.* strain SEN is inducible, Biol. Pharm. Bull. 19 (1996) 701–704.
[28] T. Akao, T. Akao, K. Mibu, et al., Enzymatic reduction of sennidin and sennoside in *Peptostreptococcus intermedius*, J. Pharmacobiodyn. 8 (1985) 800–807.
[29] M. Dreessen, H. Eyssen, J. Lemli, The metabolism of sennosides A and B by the intestinal microflora: in vitro and in vivo studies on the rat and the mouse, J. Pharm. Pharmacol. 33 (1981) 679–681.
[30] Z. Huang, Y. Xu, Q. Wang, et al., Metabolism and mutual biotransformations of anthraquinones and anthrones in rhubarb by human intestinal flora using UPLC-Q-TOF/MS, J. Chromatogr. B Analyt. Technol. Biomed. Life Sci. 1104 (2019) 59–66.
[31] H.W. Kavunja, K.J. Biegas, N. Banahene, et al., Photoactivatable glycolipid probes for identifying mycolate-protein interactions in live mycobacteria, J. Am. Chem. Soc. 142 (2020) 7725–7731.
[32] W. Li, Y. Zhou, W. You, et al., Development of photoaffinity probe for the discovery of steviol glycosides biosynthesis pathway in *Stevia rebuadiana* and rapid substrate screening, ACS Chem. Biol. 13 (2018) 1944–1949.
[33] Y.S. Keum, Y.H. Han, C. Liew, et al., Induction of heme oxygenase-1 (HO-1) and NAD[P]H: Quinone oxidoreductase 1 (NQO1) by a phenolic antioxidant, butylated hydroxyanisole (BHA) and its metabolite, tert-butylhydroquinone (tBHQ) in primary-cultured human and rat hepatocytes, Pharm. Res. 23 (2006) 2586–2594.
[34] X. Zhang, T. Yu, C. Liu, et al., Cysteine reduced the inhibition of CO_2 on heterotrophic denitrification: Restoring redox balance, facilitating iron acquisition and carbon metabolism, Sci. Total Environ. 826 (2022), 154173.
[35] A. Bansal, M.C. Simon, Glutathione metabolism in cancer progression and treatment resistance, J. Cell Biol. 217 (2018) 2291–2298.
[36] A. Aguilera, F. Berdun, C. Bartoli, et al., C-ferroptosis is an iron-dependent form of regulated cell death in cyanobacteria, J. Cell Biol. 221 (2022), e201911005.
[37] A.M. Distéfano, M.V. Martin, J.P. Córdoba, et al., Heat stress induces ferroptosis-like cell death in plants, J. Cell Biol. 216 (2017) 463–476.
[38] J.D. Hardcastle, J.L. Wilkins, The action of sennosides and related compounds on human colon and rectum, Gut 11 (1970) 1038–1042.
[39] M. Matsumoto, A. Ishige, Y. Yazawa, et al., Promotion of intestinal peristalsis by *Bifidobacterium* spp. capable of hydrolysing sennosides in mice, PLoS One 7 (2012), e31700.
[40] M. Hattori, T. Namba, T. Akao, et al., Metabolism of sennosides by human intestinal bacteria, Pharmacology 36 (1988) 172–179.
[41] M. Hattori, G. Kim, S. Motoike, et al., Metabolism of sennosides by intestinal flora, Chem. Pharm. Bull. (Tokyo) 30 (1982) 1338–1346.
[42] M. Dreessen, J. Lemli, Qualitative and quantitative interactions between the sennosides and some human intestinal bacteria, Pharm. Acta Helv. 57 (1982) 350–352.
[43] L. Zhang, W. Bao, R. Wei, et al., Inactivating NADH:quinone oxidoreductases affects the growth and metabolism of *Klebsiella pneumoniae*, Biotechnol. Appl. Biochem. 65 (2018) 857–864.
[44] F.V. Sena, F.M. Sousa, A.S.F. Oliveira, et al., Regulation of the mechanism of type-II NADH: Quinone oxidoreductase from *S. aureus*, Redox Biol. 16 (2018) 209–214.
[45] J.A. Quaye, J. Ball, G. Gadda, Kinetic solvent viscosity effects uncover an internal isomerization of the enzyme-substrate complex in *Pseudomonas aeruginosa* PAO1 NADH:Quinone oxidoreductase, Arch. Biochem. Biophys. 727 (2022), 109342.
[46] A. Dibrov, M. Mourin, P. Dibrov, et al., Molecular dynamics modeling of the *Vibrio cholera* Na^+-translocating NADH: Quinone oxidoreductase NqrB-NqrD subunit interface, Mol. Cell. Biochem. 477 (2022) 153–165.
[47] J. Šileikytė, S. Sundalam, L.L. David, et al., Chemical proteomics approach for profiling the NAD interactome, J. Am. Chem. Soc. 143 (2021) 6787–6791.
[48] F. Nasher, A.J. Taylor, A. Elmi, et al., MdaB and NfrA, two novel reductases important in the survival and persistence of the major enteropathogen *Campylobacter jejuni*, J. Bacteriol. 204 (2022), e0042121.
[49] H. Andersson, E. Piras, J. Demma, et al., Low levels of the air pollutant 1-nitropyrene induce DNA damage, increased levels of reactive oxygen species and endoplasmic reticulum stress in human endothelial cells, Toxicology 262 (2009) 57–64.
[50] E. Johansson, G.N. Parkinson, W.A. Denny, et al., Studies on the nitroreductase prodrug-activating system. Crystal structures of complexes with the inhibitor dicoumarol and dinitrobenzamide prodrugs and of the enzyme active form, J. Med. Chem. 46 (2003) 4009–4020.
[51] J. Jumper, R. Evans, A. Pritzel, et al., Highly accurate protein structure prediction with AlphaFold, Nature 596 (2021) 583–589.